Direct detection and measurement of wall shear stress using a filamentous bio-nanoparticle

Lobo, Daniela; Simmons, Mark; Hicks, Matthew; Dafforn, Timothy; Arkill, Kenton; Smith, David; Little, Haydn; Pacheco-Gomez, Raul

DOI:
10.1007/s12274-015-0831-x

Document Version
Peer reviewed version

Citation for published version (Harvard):
Lobo, D, Simmons, M, Hicks, M, Dafforn, T, Arkill, K, Smith, D, Little, H & Pacheco-Gomez, R 2015, 'Direct detection and measurement of wall shear stress using a filamentous bio-nanoparticle', *Nano Research*, vol. 8, no. 10, pp. 3307-3315. https://doi.org/10.1007/s12274-015-0831-x

TABLE OF CONTENTS (TOC)

Direct detection and measurement of wall shear stress using a filamentous bio-nanoparticle

Daniela P. Lobo, Alan M. Wemyss, David J. Smith, Anne Straube, Kai B. Betteridge, Andrew H.J. Salmon, Rebecca R. Foster, Hesham E. Elhegni, Simon C. Satchell, Haydn A. Little, Raúl Pacheco-Gómez, Mark J. Simmons, Matthew R. Hicks, David O. Bates, Alison Rodger (✉), Timothy R. Dafforn, and Kenton P. Arkill

Universities of Warwick, Birmingham, Nottingham and Bristol, United Kingdom

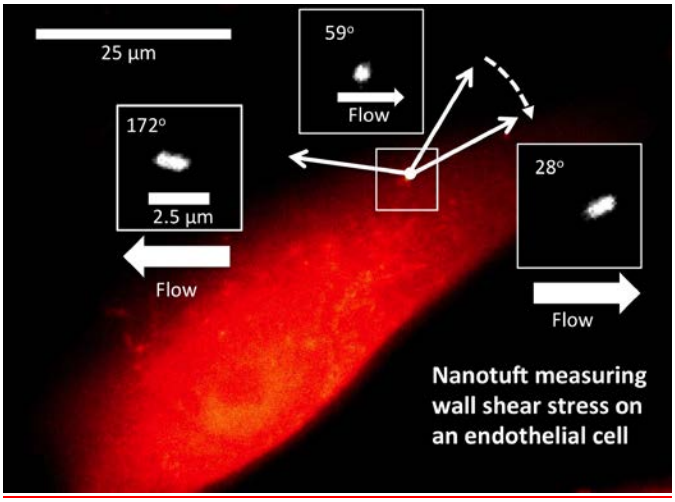

Local values of wall shear stress are determined by detecting how an anchored filamentous bacteriophage responds to flow. The nanosensor is anchored to cellular and other surfaces by targeted molecular assembly.

Provide the authors' webside if possible.

http://www2.warwick.ac.uk/fac/sci/chemistry/research/arodger/arodgergroup

http://www.birmingham.ac.uk/staff/profiles/biosciences/dafforn-tim.aspx

http://research-information.bristol.ac.uk/en/persons/kenton-arkill(c5271f31-ee5d-4b7c-9287-9e08875bec07).html

Nano Research
DOI (automatically inserted by the publisher)
Research Article
ISSN 1998-0124
CN 11-5974/O4

Direct detection and measurement of wall shear stress using a filamentous bio-nanoparticle

Daniela P. Lobo[1], Alan M. Wemyss[1,2], David J. Smith[3], Anne Straube[4], Kai B. Betteridge[5], Andrew H.J. Salmon[5], Rebecca R. Foster[6], Hesham E. Elhegni[6], Simon C. Satchell[6], Haydn A. Little[7], Raúl Pacheco-Gómez[8], Mark J. Simmons[9], Matthew R. Hicks[8], David O. Bates[1,0] Alison Rodger[1] (✉), Timothy R. Dafforn[8], and Kenton P. Arkill[11]

[1] *Department of Chemistry and Warwick Analytical Science Centre, University of Warwick, Coventry, CV4 7AL, UK*
[2] *MOAC Doctoral Training Centre, University of Warwick, Coventry, CV4 7AL, UK*
[3] *Mathematics, University of Birmingham, Edgbaston, Birmingham, West Midlands, B15 2TT, UK*
[4] *Centre for Mechanochemical Cell Biology, Warwick Medical School, University of Warwick, Coventry, CV4 7AL, UK*
[5] *Physiology and Pharmacology, University of Bristol, University Walk, Bristol, BS8 1TD, UK*
[6] *Clinical Sciences, Whitson Street, University of Bristol, Bristol BS1 3NY, UK*
[7] *School of Chemistry, University of Birmingham, Edgbaston, Birmingham, West Midlands, B15 2TT, UK*
[8] *Biosciences, University of Birmingham, Edgbaston, Birmingham, West Midlands, B15 2TT, UK*
[9] *Chemical Engineering, University of Birmingham, Edgbaston, Birmingham, West Midlands, B15 2TT, UK*
[10] *Cancer Biology, School of Medicine, University of Nottingham, Queen's Medical Centre, Nottingham NG2 7UH, UK*
[11] *Biochemistry, University of Bristol, University Walk, Bristol, BS8 1TD, UK*

Corresponding Author Alison Rodger: a.rodger@warwick.ac.uk, Phone: +442476574696

Received: day month year
Revised: day month year
Accepted: day month year (automatically inserted by the publisher)

KEYWORDS

Microfluidics, nanoparticle, M13 bacteriophage, wall shear stress, fluorescent microscopy

ABSTRACT

The wall shear stress (WSS) that a moving fluid exerts on a surface affects many processes including those relating to vascular function. WSS plays an important role in normal physiology (*e.g.* angiogenesis) and affects the microvasculature's primary function of molecular transport. It is known that points of fluctuating WSS show abnormalities in a number of diseases, however, there is no established technique for measuring WSS directly in physiological systems. All current methods rely on estimates obtained from measured velocity gradients in bulk flow data. In this work we report a nanosensor that can directly measure WSS in microfluidic chambers with sub-micron spatial resolution using a specific type of virus, the bacteriophage M13, which has been fluorescently labelled and anchored to a surface. It is demonstrated that the nanosensor can be calibrated and adapted for biological tissue, giving results that show WSS in micro-domains of cells that cannot be calculated accurately from bulk flow measurements. This method lends itself to a platform applicable to many applications in biology and microfluidics.

1 Introduction

The interaction between flowing liquids and solid surfaces, such as blood and endothelial cells, affects the function of both surface and liquid. The force per unit area that a moving fluid exerts parallel to a surface or wall is known as the wall shear stress (WSS). This parameter affects cellular and biochemical reactions and is therefore important for a range of fields, including microfluidic system design [1] and understanding disease states of the vascular system [2]. WSS plays an important role in normal physiology and affects the microvasculature's primary function of molecular transport [3-7]. It is known that points of fluctuating WSS show abnormalities in diseases such as atherosclerosis, diabetes and cancer. Measuring WSS directly is currently possible only on a relatively large scale by techniques such as microelectromechanical sensors [8] and quasi-direct methods such as deformable micropillars (a micropillar device is ~100 μm tall) [9, 10]. There is no established technique for measuring WSS directly in physiological systems. All methods rely on estimation of WSS using velocity gradients measured close to the wall, the fluid rheology, and the assumption of a boundary condition at the surface (*e.g.* the Dirichlet no-slip condition). Such methods are unreliable when applied to the circulatory system, which exhibits pulsatile three-dimensional flow containing fluid particulates and has elastic walls of varying geometries. Thus, development of new methods to measure WSS is important.

In the vasculature, the velocity gradient at the wall is currently measured by bulk flow techniques such as micro-particle image velocimetry (μPIV) [11] to calculate the velocity gradient at the wall by making assumptions including uniformity of flow and of the surface. Such an average measurement may hide variability critical to the understanding of disease states in complex, dynamic and variable systems such as a blood vessel. μPIV methods all struggle with the complex nature of blood, and are limited by the particle size used (as well as viable flow ranges). Interpreting experimental data is also dependent on the computational models (and associated assumptions) used to determine WSS in medicine [12].

Any fluid moving along a solid boundary induces a shear stress on that boundary. For a Newtonian fluid in laminar flow, such as blood plasma, the WSS is

$$WSS = \eta \left. \frac{\partial V}{\partial y} \right|_0 \quad (1)$$

where η is the dynamic viscosity of the fluid, V is its velocity, and y is the height above the boundary. The horizontal axis refers to WSS as calculated from a model of laminar flow in a smooth rectangular channel (numerical values taken from manufacturer's data). This quantity is a 'nominal' value because it does not correct for local variations such as roughness over the surfaces of cells.

Reported here is a strategy for measuring WSS using labelled M13 bacteriophage as a microfluidic reporter. Previous work has reported its use as a scaffold for nanowires [13-15] and fibers [16, 17], biosensors [18], drug delivery [19], cancer markers [20], and detection of biological molecules [18]. M13 bacteriophage (M13) is a long (~900 nm) and thin (~7 nm) semi-rigid construct whose persistence length is ~1400 nm [21]. The alignment in flow and spectroscopy of this filamentous particle has recently been exploited in our previous work for a variety of diagnostic assays [22]. We have generated chemical modification protocols to label M13 with fluorophores that provide a suite of signals detectable using linear dichroism (a differential polarized light spectroscopy technique). A number of methods have been developed to modify chemically the surface of the M13, adding an extensive list of moieties to the surface of the virus.

The M13 naturally possesses different chemical groups at each end [23]. Therefore it is theoretically possible to chemically tether one end to a surface and visualize it under various shear conditions as a nanotuft (Fig. 1). In this work we report our observations of the behavior of M13 in fluid flow, together with the chemical modification protocols developed in our laboratory [22], to produce a system that can be used to study flow at surfaces. It results in a simple, novel, scalable, synthetic biology method for measuring WSS on a sub-micron scale using fluorescent microscopy. The nanosensor is an M13 with a specific binding agent (*e.g.* an antigen-specific antibody) attached to one end *via* pIII proteins and fluorophores attached to the pVIII proteins (Fig. 1). The appropriate antigen was

attached to the surface of the flow cell and its behaviour visualised in flow. Subsequent data analysis allowed us to determine the WSS for both the collagen and cultured endothelial cells affixed to coated plastic slides. The result is a nanosensor that is potentially usable *in vivo*.

2 Experimental

Wheat germ aglutinnin (WGA) was obtained from Sigma-Aldrich, Poole, UK and the anti-collagen antibody from Abcam, Cambridge, UK. Other chemicals were obtained from the suppliers given in the Electronic Supplementary Material (ESM) and used as received unless stated otherwise. M13 bacteriophage were grown, purified, and fluorescently labelled as described in detail elsewhere [22] and outlined in the ESM. M13 was derivatised with the protein anchor attached to the pIII protein as described in the ESM. The structure of the nanosensor construct is schematically illustrated in Fig. 1(a). Collagen IV-coated microchannel plates (μ-Slide I Luer$^{0.8}$ ibidi, Munich) were assembled into a controlled flow system using a pump (ibidi, Munich). We have previously shown that ibidi systems are able to orient semi-rigid molecular systems [24]. Human conditionally immortalized glomerular endothelial cells [25] (GEnCs), were grown as described in the ESM. The completed M13 construct was bound to the flow slide coating (collagen IV or endothelial cells) and unbound M13 rinsed off.

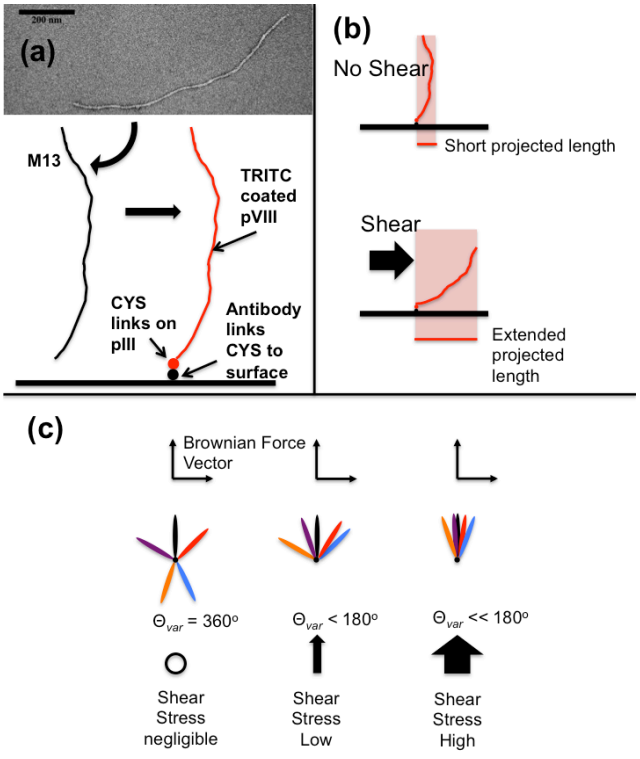

Figure 1 Principles and design of bacteriophage construct. (a) Transmission electron micrograph of M13 with uranyl acetate stain. A schematic of the M13 followed by our process of using cysteines (CYS) on the pIII to bind a molecule designed to affix the M13 to a target surface. pVIII proteins are covalently labelled with a fluorescent isothiocyaniate derivative (tetramethylrhodamine-5-(and-6)-isothiocyanate (TRITC)) for fluorescent imaging. (b) A possible method of detection by length. (c) A possible method of detection by variation in angle.

A nominal WSS (0–3.5 dyn.cm^{-2}) was applied. See ESM and the ibidi website for further details. The fluorescent images of the derivatised and labelled M13 construct in flow were measured using either spinning disk confocal microscope (Ultraview spinning disk confocal microscope with a 1.4 NA, 100× oil immersion objective, 561 nm laser, TRITC filter sets (Croma) and an ORCA R^2 camera (Hamamatsu) under control of Volocity 6.3, Perkin-Elmer) at 10 frames per second or a Nikon Ti Eclipse inverted microscope through 60× oil immersion objective 1.4 (Nikon Plan Apo VC 60x Oil DIC N2).

Recorded time-lapse images of collagen-coated slides were post-analysed using a bespoke function in MATLAB 2014b (MATLAB R2014b, The MathWorks Inc., Natick, MA). Videos and more

details are available in the ESM.

The analysis allowed the determination of the orientation angle and approximate length and width of the M13 nanosensor in each frame. Using MATLAB the region that the M13 occupies on each frame is first defined by finding a threshold pixel intensity below which all pixels were set to zero, and above which they were set to one (Otsu method [26]). The pixels with value one whose nearest neighbor also had value one were then defined as regions of interest (ROI). The largest of these is assumed to be the M13. An image stack with the largest ROI subtracted out is created to be the background that is subtracted from the original binary image, leaving only a M13 nanosensor in each image. To smooth the edges of this ROI and fill any pixels of zero intensity in its interior – both of which would affect subsequent analysis – a convex polygon was fitted to the ROI. The major axis was then defined as the longest possible straight line that could be drawn within the ROI, and its angle determined relative to the horizontal axis of the image defined the bacteriophage's orientation. The directionality plugin in Fiji/ImageJ [27] gave comparable results.

The tethered nano-particle motion under Brownian effects and flow was modeled phenomenologically by a random walk with spatially homogeneous jump probability, but a spatially-varying difference in the probability of left or right jumps, modeling the biasing effect of the viscous restoring force as described in the ESM.

3 Results and discussion

3.1 Production and microscopy of labelled and derivatised nanosensors

Two systems were developed using a novel M13 nanosensor to determine WSS.

(i) Fluorescent M13 constructs derivatised with anti-collagen IV antibodies (M13-aCol-TRITC) attached to a collagen IV-coated microchannel plate substrate. The collagen IV was designed to act as a relatively flat surface to test the principles of the nanosensor.

(ii) Fluorescent M13 constructs derivatised with WGA (M13-WGA-TRITC) attached to cultured endothelial cells (GEnCs) *via* the glycoclayx (WGA binds to sialic acid reidues on the surface of glycoproteins that form the gycocalyx on most endothelial cells). The endothelial cells were designed to act as a model blood vessel.

3.2 Detection of WSS on collagen coated slides

Spinning disc images of M13-aCol-TRITC exposed to a range of nominal WSS (0–3.5 dyn.cm^{-2}) were collected. The data from these experiments take the form of time-lapse images of individual M13-aCol-TRITC constructs on the surface. The constructs could be recognized under the microscope as bright points, agitating in the buffer. Once under high digital magnification, the M13-aCol-TRITC appear as elliptical shapes, due to the diffraction limit of light, that adopt different angles as a function of time (Fig. 2(a)). Fourteen independent M13-aCol-TRITC data sets were collected at each flow condition. Once an M13-aCol-TRITC was in focus, then flow was induced to test if the construct was bound. Images of the flow slide with no shear flow applied suggested that the M13-aCol-TRITC construct is on the surface and oriented in random fashion (in response to Brownian motion, Fig. 2(c). The reaction to flow-induced shear is obvious by eye: the fluorescent ellipse orients, seemingly instantaneously, with its long axis preferentially aligned with the shear flow direction. The degree of orientation increases with flow rate. The microscope focus typically required adjustment to achieve optimal imaging. The signal to noise decreased overtime as would be expected if bleaching was occurring, however, more than 10 minutes of continuous imaging was possible with both the spinning disk confocal and widefield microscopes. An example of a M13-aCol-TRITC video is available in the ESM.

3.3 Measurement of WSS on GEnCs

Human conditionally immortalised glomerula endothelieal cells (GEnCs), normally used as a model capillary system for kidney disease, were seeded onto sterile, collagen-coated flow slides because these kidney-derived cells provide an intellectual bridge to future work on how complications of diabetes (*e.g.* nephropathy) affects flow in kidneys. WGA conjugated to the pIII protein of M13 (M13-WGA-TRITC) made a body that was visualised using a wide-field fluorescent microscope showing that the bacteriophage had successfully adhered to

cells on the flow slide surface (Fig. 2(b)) and had formed a confluent layer.

Time-lapsed images show that in the absence of flow the conjugates move fairly randomly in response to Brownian motion in a manner consistent with it being attached to the cellular surface only at one end, however, the angle space it explores is reduced compared with the collagen-only slides (Fig. 2(c) and 2(d)) and the mean angles in both negative and positive flow directions are non zero, in contrast to the collagen surfaces. This suggests the bacteriophage is located on the side of a cell, near the top, with the cell surface forcing minimum angles of approximately –10° for negative flow and +30° for positive flow.

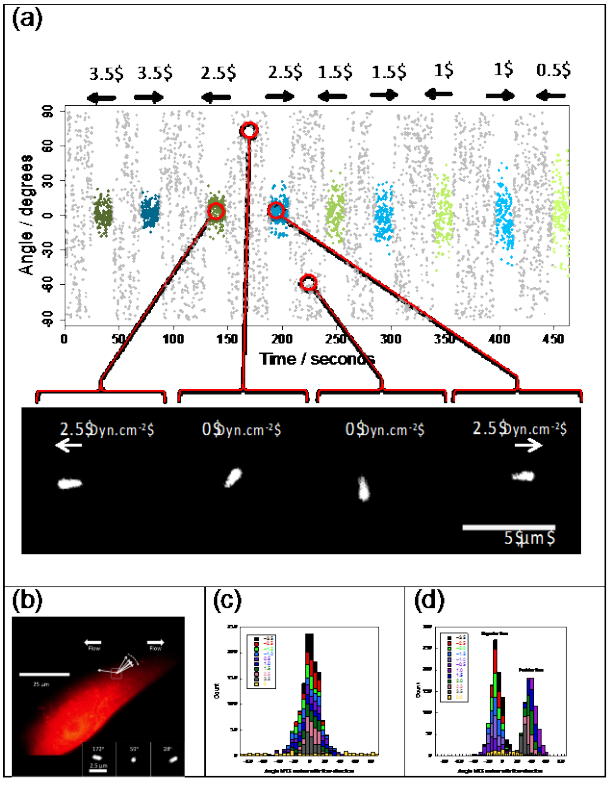

Figure 2 (a) Example of wall shear stress visualized by M13-aCol-TRITC bound to a collagen IV coated flow slide. M13 orientation versus time in a typical experiment. The nominal wall shear stress (assuming a linear relationship between bulk fluid flow and WSS) is indicated at the top in dyn.cm^{-2}. The flow direction and magnitude at each time point are indicated by the arrows and by the colour and intensities of the overlays (negative (blue), positive (green) and zero (grey)). Example images as time points corresponding to the red circles in of background subtracted spinning disk confocal image frames are shown below. (b) Wall shear stress effect on a M13-WGA-TRITC bound to the surface of a cultured GEnCs with inset of snapshots of three flows, giving the indicated nominal wall shear stress and the average orientation. Additive histograms for the angles a bound M13 makes with (c) a collagen-only coated slide and (d) a surface layered with GEnCs.

3.4 Quantitation of response of M13-aCol-TRITC construct to flow and WSS

To use the above data to quantify WSS a robust data analysis methodology was required. This has two parts.

Turning the videos into orientation data of the type summarized in Fig. 2(a)

A MATLAB code was written to extract the bacteriophage orientation and major axis length data. Its angle relative to the horizontal axis of the image defined the bacteriophage's orientation as summarized in Fig. 2(a) and 2(c). The MATLAB segmentation code was found to be accurate by eye and gave similar results to the imageJ directionality pluggin. A video comparison is shown in ESM video 2. Both methods gave erratic readings when there was poor focus or other poor signal to noise ratio situations. Also if the M13 appeared round (due to pointing straight up) the angles derived were erratic by both methods.

Development of a theoretical model of how the bacteriophage orientation relates to the flow

Both the apparent mean length of the bacteriophage and the variation of its orientation in flow will depend on the shear stress it experiences. If a theoretical model is to be of any use it must be consistent with the experimental data. The maximum mean length in most examples was ~1.3 µm, which is consistent with the expected length plus the expected Airy disk, indicating the M13 is almost parallel to the surface at maximum flow, and decreases with flow velocity. There was a correlation between length and nominal WSS, however, as there are only a few pixels between maximum and minimum lengths the resolution was too low for WSS measurement. Fortunately, the variation in angle showed more resolution.

A simple two dimensional random walk model predicts a normal distribution of angle about a mean direction with the logarithm of the standard

deviation of the angle (σ) being linearly related to the logarithm of the WSS, with a slope of 0.5 (see ESM)

$$\ln(\sigma) = -0.5\ln(WSS) - 1.5\ln(L) + k \quad (2)$$

where L is the particle length and k is a constant. The data in Fig. 3(a) (Run A) and 3(b) (collagen combined data) for 5 independent runs of an M13 bacteriophage anchored onto a collagen-coated flat slide are in accord with such a model, where WSS on the horizontal axis is a nominal value calculated from bulk flow rates (see ESM). The GEnC data (Fig. 3(a)) are also consistent with the model within the larger experimental error of these experiments. Better statistics, either from a higher frame rate, longer runs, or more bacteriophage would be desirable.

The scatter plots of Fig. 3(c) show clearly the different behaviour of the flat collagen coated slides and the two opposite flow directions of the GEnC coated slides: the flow direction has no significant effect on the average M13-aCol-TRITC angle or the standard deviation of its observed angles for the collagen coated slides but a significant effect on both the average angle, and standard deviation of angles of the GEnC slides. The reduced angle space of the GEnC data sets (Fig. 2(d)) may suggest some degree of non-specific interaction of M13 with the cell surface. However, the space sampled in zero flow is still bigger than at the lowest flow rates, so these interactions will not significantly affect the analysis.

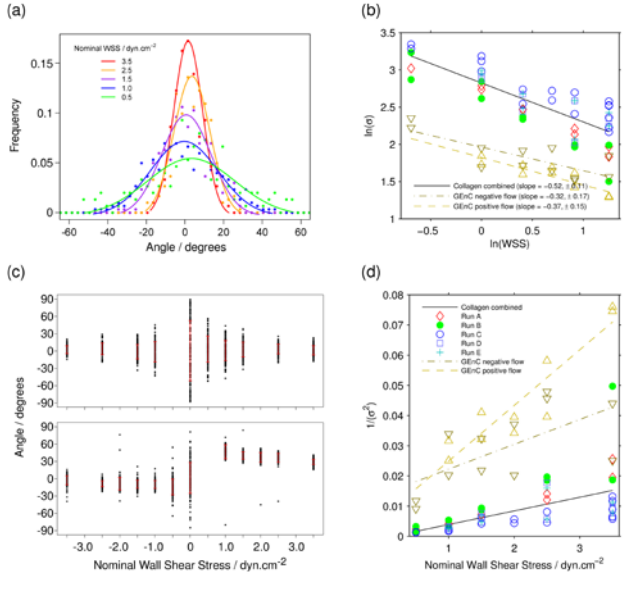

Figure 3 (a) The normalized frequency distribution of angles for an M13 bacteriophage anchored to a collagen coated slide with a Gaussian fit to the original data points (Run A in Figure 3(b)) as a function of nominal-flow-induced-WSS in dyn.cm^{-2}. (b) ln(σ) versus ln(nominal WSS) for 5 measured M13-aCol-TRITC movies and one GEnC movies all involving both positive and negative direction flows, for σ the standard deviation of the angle at each flow rate. (c) Orientation versus nominal WSS for an M13 anchored to collagen (top) and GEnC coated slides (bottom), negative flow left, positive flow right. σ is denoted by the bold red bar for each flow. (d) Plots of inverse variance versus nominal WSS for the data plotted in and (b). Quoted errors on the slopes are 95% confidence intervals of the fit to a straight line.

Although the x-intercepts of the ln/ln plots of Fig. 3(b) contain the information to determine the true WSS from ln(σ) and ln(nominal WSS), the error in the intercept is large. So instead Eq. (3) was plotted.

$$\frac{1}{\sigma^2} \propto \text{Nominal WSS} \quad (3)$$

Nominal WSS is the value of the WSS if the bulk flow is a correct predictor of the flow at the surface. We expect this to be accurate for the collagen experiments. By way of contrast, even though the slopes of the two GEnC lines in Fig. 3(d) have a large error, they are clearly larger than those of the collagen-coated slides indicating that the bulk-flow-determined nominal WSS is not a good estimate of WSS at the cell surface. The slopes of Fig. 3(d) suggest that the negative flow direction has WSS of more than twice the nominal value, and the positive direction over three times the nominal value.

The μ-slide is approximately 80× deeper than the cell so the enhanced WSS of the GEnC experiments effect is unlikely to be from channel narrowing. Various other factors presumably contribute to the observation, including roughness of the surface, local viscosity effects, and the shape of the protrusion into the μ-slide. Barbee *et al.* [28] measured the height of endothelial cells above a surface using atomic force microscopy and approximated the shear stress due to flow across the surface through a simplified computational fluid dynamics approach: their result suggest approximately 50% enhancement of WSS due to the shape protrusion of the cells. Pozrikidis [29] mathematically modelled flow over protuberances on a plane wall: for an elongated hemispheroid with an aspect ratio of 0.2 (similar to the [28] cells) WSS was calculated to increase by 1.5×; for an aspect ratio of 0.5 this factor increased to 2.5×. Thus much of the increase in WSS with our GEnC

experiments is due to the shape of the cells compared with the flat collagen slides, however, other factors are also playing a role and show the importance of being able to measure WSS locally.

4 Conclusion

WSS is usually calculated using flow velocity gradients measured close to the wall with boundaries and Newtonian assumptions that are often an approximation. Here we have shown that by anchoring one end of a fluorescent M13 bacteriophage onto surfaces, when directional flow is applied, the free body of the nanoreporter repositions resulting in a novel nanosenor that can be used to measure WSS with a 1 μm spatial resolution which is 100× better than currently implemented methods.

We calibrated the approach with a model system to show we could predict the relationship, using a simple theoretical model, between particle flow behaviour and WSS. We have then been able to measure local WSS of the irregular surface of a cultured cell proving the concept and showing that the normal predictions by bulk flow cannot be relied upon. The system is adaptable and can in principle be used in *in vivo* systems as it requires only wide-field fluorescent microscopy. The technique and production methodology have been demonstrated on two types of surface: relatively flat collagen coated slides, which compare well with bulk flow expectations, and an endothelial cell coated surface which show higher WSS than bulk flow values. Our data therefore suggest that WSS operative in physiological systems is likely to deviate significantly from that expected based on bulk flow estimates.

There are several key areas to develop, none of which we believe are insurmountable, before the technique can be used in earnest *in vitro* or *in vivo* to explore how differences in cell surfaces are affected by local flow effects. The physical properties of the nanofiber-cell binding, in particular its compliance, may affect the precise details of the response to shear. However, provided that the fibre is able to undergo relatively free rotation as exhibited in the present data, the balance between Brownian rotation and shear flow deflection will provide a sensitive and accurate indication of WSS once calibrated to the particular construct.

In summary, although further construct and data-quality development are needed, this bacteriophage construct, with low manufacturing costs and high adaptability, suggests a way forward to map flow and WSS on the micron scale in biological systems thus opening up a wide range of potential applications in fundamental research and diagnosis.

Acknowledgements

The technical expertise of Ian Hands-Portman at the Imaging Suite, of Life Sciences, University of Warwick, Coventry, CV4 7AL contributed significantly to this work. The funding from a variety of sources to support this work is gratefully acknowledged: Engineering and Physical Sciences Research Council (Impact Acceleration Account EP/K503873/1: MJS, KPA, TRD, MRH); European Union FP7 Marie Curie Initial Training Network (Innovative Doctoral Programme: DPL, AR); The Science City Research Alliance (KPA); Engineering and Physical Sciences Research Council (MOAC Doctoral Training Centre, EP/F500378/1: AW); Medical Research Council (G0802829; AHJS, KBB); British Heart Foundation (FS/10/017/28249, RRF; FS/13/42/30377: AHJS) and the Libyan higher education ministry (No: 9139, HEE).

Electronic Supplementary Material: Protocols, the basis of the theoretical analysis used, and time-lapses of the figures are available in the online version of this article at http://dx.doi.org/10.1007/s12274-***-****-*

References

[1] Nge, P. N. Rogers, C. I. Woolley, A. T. Advances in microfluidic materials, functions, integration, and applications. *Chem. Rev.* **2013**, *113*, 2550-2583.

[2] Zarins, C. K. Giddens, D. P. Bharadvaj, B. K. Sottiurai, V. S. Mabon, R. F. Glagov, S. Carotid bifurcation atherosclerosis quantitative correlation of plaque localization with flow velocity profiles and wall shear-stress. *Circ. Res.* **1983**, *53*, 502-514.

[3] Chatzizisis, Y. S. Coskun, A. U. Jonas, M. Edelman, E. R. Feldman, C. L. Stone, P. H. Role of endothelial shear stress in the natural history of coronary atherosclerosis and vascular remodeling: molecular, cellular, and vascular behavior. *J. Am. Coll. Cardiol.* **2007**, *49*, 2379-9233.

[4] Katritsis, D. Kaiktsis, L. Chaniotis, A. Pantos, J. Efstathopoulos, E. P. Marmarelis, V. Wall shear stress: theoretical considerations and methods of measurement. *Prog.*

Cardiovasc. Dis. **2007**, *49*, 307-329.
[5] Reneman, R. S. Hoeks, A. P. G. Wall shear stress as measured in vivo: consequences for the design of the arterial system. *Med. Biol. Eng. Comput.* **2008**, *46*, 499-507.
[6] Reneman, R. S. Arts, T. Hoeks, A. P. G. Wall shear stress-an important determinant of endothelial cell function and structure-in the arterial system *in vivo*. *J. Vasc. Res.* **2006**, *43*, 251-269.
[7] Young, E. W. K. Beebe, D. J. Fundamentals of microfluidic cell culture in controlled microenvironments. *Chem. Soc. Rev.* **2010**, *39*, 1036-1048.
[8] Naughton, J. W. Sheplak, M. Modern developments in shear-stress measurement. *Prog. Aerosp. Sci.* **2002**, *38*, 515-570.
[9] Große, S. Schröder, W. Mean wall-shear stress measurements using the micro-pillar shear-stress sensor MPS3. *Meas. Sci. Technol.* **2008**, *19*, 015403.
[10] Brücker, C. Spatz, J. Schröder, W. Feasability study of wall shear stress imaging using microstructured surfaces with flexible micropillars. *Exp. Fluids.* **2005**, *39*, 464-474.
[11] Smith, M. L. Long, D. S. Damiano, E. R. Ley, K. Near-wall mu-PIV reveals a hydrodynamically relevant endothelial surface layer in venules *in vivo*. *Biophys. J.* **2003**, *85*, 637-645.
[12] Samady, H. Eshtehardi, P. McDaniel, M. C. Suo, J. Dhawan, S. S. Maynard, C. Timmins, L. H. Quyyumi, A. A. Giddens, D. P. Coronary artery wall shear stress is associated with progression and transformation of atherosclerotic plaque and arterial remodeling in patients with coronary artery disease. *Circulation* **2011**, *124*, 779-788.
[13] Mao, C. Solis, D. J. Reiss, B. D. Kottmann, S. T. Sweeney, R. Y. Hayhurst, A. Georgiou, G. Iverson, B. Belcher, A. M. Virus-based toolkit for the directed synthesis of magnetic and semiconducting nanowires. *Science* **2013**, *303*, 213-217.
[14] Murugesan, M. Abbineni, G. Nimmo, S. L. Cao, B. Mao, C. Virus-based photo-responsive nanowires formed by linking site-directed mutagenesis and chemical reaction. *Sci. Rep.* **2013**, *3*, 1820.
[15] Nam, K. T. Kim, D. W. Yoo, P. J. Chiang, C. Y. Meethong, N. Hammond, P. T. Chiang, Y. M. Belcher, A. M. Virus-enabled synthesis and assembly of nanowires for lithium ion battery electrodes. *Science* **2006**, *312*, 885-888.
[16] Chiang, C. Y. Mello, C. M. Gu, J. Silva, E. C. C. M. Van Vliet, K. J. Belcher, A. M. Weaving Genetically Engineered Functionality into Mechanically Robust Virus Fibers. *Adv. Mater.* **2007**, *19*, 826-832.
[17] Niu, Z. Bruckman, M. A. Harp, B. Mello, C. M. Wang, Q. Bacteriophage M13 as a scaffold for preparing conductive polymeric composite fibers. *Nano Res.* **2008**, *1*, 235-241.
[18] Domaille, D. W. Lee, J. H. Cha, J. N. High density DNA loading on the M13 bacteriophage provides access to colorimetric and fluorescent protein microarray biosensors. *Chem. Commun.* **2013**, *49*, 1759-1761.
[19] Suthiwangcharoen, N. Li, T. Li, K. Thompson, P. You, S. Wang, Q. M13 bacteriophage-polymer nanoassemblies as drug delivery vehicles. *Nano Res.* **2011**, *4*, 483-493.
[20] Carrico, Z. M. Michelle E. Farkas, M. E. Zhou, Y. Hsiao, S. H. Marks, J. D. Chokhawala, H. Clark, D. S. Francis, M. B. N-terminal labelling of filamentous phage to create cancer marker imaging agents. *ACS Nano* **2012**, *6*, 6675-6680.
[21] Khalil, A. S. Ferrer, J. M. Brau, R. R. Kottmann, S. T. Noren, C. J. Lang, M. J. Belcher, A. M. Single M13 bacteriophage tethering and stretching. *Proc. Nat. Acad. Sci. USA* **2007**, *104*, 4892-4897.
[22] Pacheco-Gomez, R. Kraemer, J. Stokoe, S. England, H. J. Penn, C. W. Stanley, E. Rodger, A. Ward, J. Hicks, M. R. Dafforn, T. R. Detection of Pathogenic Bacteria Using a Homogeneous Immunoassay Based on Shear Alignment of Virus Particles and Linear Dichroism. *Anal. Chem.* **2012**, *84*, 91-97.
[23] Sidhu, S. S. Engineering M13 for phage display. *Biomol. Eng.* **2001**, *18*, 57-63
[24] Cheng, X. Joseph, M. B. Covington, J. A. Dafforn, T. R. Hicks, M. R. Rodger, A. Continuous-channel flow linear dichroism. *Anal. Methods* **2012**, *4*, 3169-3173.
[25] Satchell, S. C. Tasman, C. H. Singh, A. Ni, L. Geelen, J. von Ruhland, C. J. O'Hare, M. J. Saleem, M. A. van den Heuvel, L. P. Mathieson, P. W. Conditionally immortalized human glomerular endothelial cells expressing fenestrations in response to VEGF. *Kidney Int.* **2006**, *69*, 1633-1640.
[26] Otsu, N. A threshold selection method from gray-level histogram. *IEEE T. Syst. Man CY.* **1979**, *9*, 62-66.
[27] Schindelin, J. Arganda-Carreras, I. Frise, E. K., V. Longair, M. Pietzsch, T. Preibisch, S. Rueden, C. Saalfeld, S. Schmid, B. Tinevez, J.-Y. White, D. J. Hartenstein, V. Eliceiri, K. Tomancak, P. Cardona, A. Fiji: an open-source platform for biological-image analysis. *Nat. Methods* **2012**, *9*, 676-682.
[28] Barbee, K. A. Mundel, T. Lal, R. Davies, P. F. Subcellular distribution of shear stress at the surface of flow-aligned and nonaligned endothelial monolayers. *Am. J. Physiol-Heart C.* **1995**, *268*, H1765-H1772.
[29] Pozrikidis, C. Shear flow over a protuberance on a plane wall. *J. Eng. Math.* **1997**, *31*, 29-42.
[30] Arkill, K. P. Neal, C. R. Mantell, J. M. Michel, C. C. Qvortrup, K. Rostgaard, J. Bates, D. O. Knupp, C. Squire, J. M. 3D Reconstruction of the Glycocalyx Structure in Mammalian Capillaries using Electron Tomography. *Microcirculation* **2012**, *19*, 343-351.

Electronic Supplementary Material

Direct detection and measurement of wall shear stress using a filamentous bio-nanoparticle

Daniela P. Lobo[1], Alan M. Wemyss[1,2], David J. Smith[3], Anne Straube[4], Kai B. Betteridge[5], Andrew H.J. Salmon[5], Rebecca R. Foster[6], Hesham E. Elhegni[6], Simon C. Satchell[6], Haydn A. Little[7], Raúl Pacheco-Gómez[8], Mark J. Simmons[9], Matthew R. Hicks[8], David O. Bates[1,0] Alison Rodger[1] (✉), Timothy R. Dafforn[8], and Kenton P. Arkill[11]

Department of Chemistry and Warwick Analytical Science Centre, University of Warwick, Coventry, CV4 7AL, UK
[2] MOAC Doctoral Training Centre, University of Warwick, Coventry, CV4 7AL, UK
[3] Mathematics, University of Birmingham, Edgbaston, Birmingham, West Midlands, B15 2TT, UK
[4] Centre for Mechanochemical Cell Biology, Warwick Medical School, University of Warwick, Coventry, CV4 7AL, UK
[5] Physiology and Pharmacology, University of Bristol, University Walk, Bristol, BS8 1TD, UK
[6] Clinical Sciences, Whitson Street, University of Bristol, Bristol BS1 3NY, UK
[7] School of Chemistry, University of Birmingham, Edgbaston, Birmingham, West Midlands, B15 2TT, UK
[8] Biosciences, University of Birmingham, Edgbaston, Birmingham, West Midlands, B15 2TT, UK
[9] Chemical Engineering, University of Birmingham, Edgbaston, Birmingham, West Midlands, B15 2TT, UK
[10] Cancer Biology, School of Medicine, University of Nottingham, Queen's Medical Centre, Nottingham NG2 7UH, UK
[11] Biochemistry, University of Bristol, University Walk, Bristol, BS8 1TD, UK

Corresponding Author Alison Rodger: a.rodger@warwick.ac.uk, Phone: +442476574696

Supporting information to DOI 10.1007/s12274-****-****-* (automatically inserted by the publisher)

Production of M13 bacteriophage

M13 bacteriophage (M13) has a mono-dispersed, fibre morphology, with a well-defined semi-rigid shape, being 7 nm wide by 900 nm long. It has five structural proteins: 1 major coat protein, the pVIII, capped with 4 minor coat proteins, pIII and pVI, pVII and pIX, on the proximal and distal ends, respectively. These proteins can be chemically modified in a site-specific fashion, without disrupting its functionality [1]. M13 was produced as per the method of Pacheco-Gomez *et al.* [2] which involved the following.

A 250 mL flask containing 50 mL autoclaved NB2 (Oxoid) medium with tetracycline at 5 μg/mL (added to ensure the *Escherichia coli* used for propagating M13 maintain the F′ plasmid encoding the pilus structure, since it is required for the infection to occur) was inoculated with 50 μL of One Shot Top10F′ (Invitrogen). The culture was incubated overnight at 37 °C and 200 rpm. A volume of 40 mL of the overnight *Escherichia coli* culture was transferred into 400 mL autoclaved NB2 medium and allowed to equilibrate at 37 °C. The culture was then inoculated with M13, and incubated overnight at 37 °C and 200 rpm. The next day, the samples were centrifuged at 8000g. The supernatant containing M13 was mixed with PEG6000 and NaCl (2.5 M) to precipitate the bacteriophage particles. These were then collected by centrifugation of the samples at 8000*g* for

20 min. The supernatant was removed, and the pellet was re-suspended in 50 mM phosphate buffer, pH 8.

Caesium chloride purification of M13 bacteriophage

To purify the M13, the supernatant was mixed with caesium chloride powder to give a final concentration of 0.4 mg/mL of CsCl. The samples were centrifuged for 24 h at 35,000 rpm in 70.1 Ti rotor at 15°C. After extraction, the samples were dialysed using 3500 MWCO dialysis tubing (Sigma-Aldrich) in 50 mM potassium phosphate buffer pH 8 for 24 h.

Measurement of M13 bacteriophage concentration

M13 concentration was determined from its absorption spectrum measured using a JASCO V550 UV/Vis spectrometer. The concentration of M13 (in mg/cm^3) was then calculated based on its absorbance at 269 nm (using ε = 3.84 cm^2/mg) using the Beer-Lambert law.

Bioconjugation of M13 bacteriophage pIII protein with anti-collagen IV antibody

Anti-collagen IV antibodies (aCol) were selectively conjugated to the 5 copies of pIII, at one end of the M13, by first using mild conditions to reduce partially the disulfide bonds of the pIII protein. A 2000 molar tris(2-carboxyethyl)phosphine (TCEP Sigma-Aldrich) excess in phosphate buffer pH 7.5 (0.21 mg) was added to an initial mass of M13 (1.24 mg, 7.25×10^{-8} mmoles) in order to originate partially reduced pIII proteins (3.63×10^{-8} mmoles). The sample was incubated for 5 minutes at room temperature. The partially reduced M13 was separated from low molecular mass byproducts using a PD-10 column (Sephadex G-25, GE Healthcare), with a conjugation buffer (50 mM potassium phosphate buffer, 150 mM NaCl, 5 mM EDTA buffer, pH 7.0) as eluent. The aCol was then derivatised with maleimide. 0.05 mL of aCol (abcam, ab19808) were required in order to provide a 1:1 ratio (3.63×10^{-7} mmoles) over the pIII protein. Succinimidyl-4-(*N*-maleimidomethyl cyclohexane-1-carboxylate (0.0012 mg, SMCC, Thermo Fisher Scientific) was added to the aCol in a 10:1 molar excess (0.0012 mg). The sample was incubated for 1 h and eluted in the conjugation buffer to remove low molecular mass byproducts using a PD-10 column (Sephadex G-25, GE Healthcare). Finally, the maleimide derivatised aCol and the partially reduced M13 were mixed and left to react for 1 h before gently stirring overnight at 4 °C. *N*-ethylmaleimide (NEM, Sigma-Aldrich) was then added to the mixture (0.90 mg) in order to produce a 20000 molar excess over the pIII protein. The sample was left to react at room temperature (RT) for 15 minutes and was later purified using PD-10 columns (Sephadex G-25, GE Healthcare) in conjugation buffer.

Bioconjugation of M13 bacteriophage pIII protein with wheat germ agglutinin (WGA)

The disulfide bonds of the pIII protein (3.75×10^{-7} mmoles) were reduced using 0.5 M TCEP in phosphate buffer pH 7.5, added to an initial mass of M13 (1.28 mg, 7.5×10^{-8} mmoles). The sample was incubated for 5 minutes at RT. The partially reduced M13 was separated from low molecular mass byproducts using a PD-10 column, with a conjugation buffer (50 mM potassium phosphate buffer, 150 mM NaCl, 5 mM EDTA buffer, pH 7.0) as eluent. The WGA was then derivatised with maleimide. 2.5 mg of WGA (lectin from *Triticum vulgaris*, lyophilized powder, Sigma-Aldrich) in PBS pH 7 was used at molar equivalents to the pIII proteins. A 10× excess 1.5 mM SMCC (2.5 μL) in phosphate buffer was added. The sample was incubated for 1 h and eluted in the conjugation buffer to remove low molecular mass byproducts using a PD-10 column. These products were then mixed and left to react for 1 h before gently stirring overnight at 4 °C. 940 μL of a 1 mg/ml solution of NEM in conjugation buffer was then added to the mixture. The sample was left to react at RT for 15 minutes and was later purified using PD-10 columns (Sephadex G-25, GE Healthcare) in conjugation buffer.

Fluorescent labelling of M13 bacteriophage pVIII protein with TRITC

The pVIII proteins of the protein-derivatised M13 were then labeled with tetramethylrhodamine-5-(and-6)-isothiocyanate (TRITC, Life Technologies). TRITC is an amine-reactive dye that produced a bright orange-red fluorescent bioconjugate with excitation/emission maxima at 555/580 nm. TRITC (9.73 μL of a 10 mg/mL solution) in dimethyl sulfoxide (DMSO, Thermo Fisher Scientific) was slowly added to the M13 in 50 mM potassium phosphate buffer, pH 8.0 in order to provide a 1:1 ratio over the amine groups of the pVIII proteins (it is assumed that there are 2700 copies of this protein per M13 particle) of which there are 2 per pVIII protein (2.43×10^{-4} mmoles), the N-terminus and lysine residues. The sample was then incubated at RT, with continuous stirring for 20 h. Both constructs, M13-aCol-TRITC and M13-WGA-TRITC, were separated from unreacted TRITC using PD-10 columns, eluting the samples in conjugation buffer.

Purification and quantification of the constructs M13-antibody-TRITC and M13-WGA-TRITC

Both constructs, the M13- aCol-TRITC and the M13-WGA-TRITC, were purified using a ÄKTA Explorer 10 purification system (GE Healthcare), fitted with a Superdex 200 (120 mL column volume) HiLoad 16/60 prepacked column. The column was equilibrated with 1 column volume of water and 1.2 column volumes of elution buffer (50 mM potassium phosphate buffer, 150 mM NaCl, pH 8) before sample injection. Three wavelengths were recorded simultaneously (269 nm, 280 nm and 556 nm). 2 mL fractions were collected using a Frac-950 fraction collector (Amersham Pharmacia Biotech).

Growth of endothelial cells

Primary culture human glomerular endothelial cells were conditionally immortalized using a temperature-sensitive simian virus 40 large tumor antigen (SV40LT) construct which allows proliferation at a permissive temperature of 33 °C, and it is switched off by transfer to a non-permissive temperature of 37 °C. At this temperature, cells take on a mature phenotype [3]. GEnC were used for experiments after they were maintained at the non-permissive temperature for 4/5 days. Cells were grown in endothelial growth medium (EGM-2MV, Lonza). For experiments cells were seeded into μ-Slide I Luer$^{0.8}$ collagen coated slides (ibidi).

Imaging collagen-coated slides

The images were acquired at 10 frames per second using an Ultraview spinning disk confocal microscope with a 1.4 NA, 100× oil immersion objective, 561 nm laser, TRITC filter sets (Croma) and an ORCA R^2 camera (Hamamatsu) under control of Volocity 6.3 (Perkin-Elmer).

Imaging endothelial cell-coated slides

The M13 on the cells were visualised using a Nikon Ti Eclipse inverted microscope through 60× oil immersion objective 1.4 (Nikon Plan Apo VC 60x Oil DIC N2). Cells within the imaging window were illuminated at 535 nm using a widefield fluorescent light emitting diode (Precise Excite Cool LED) and emitted light was filtered through a 620 nm filter block and detected on a high resolution 14-bit monochromatic camera (Photometric's CoolSnap HQ2). The imaging window yielded 1392 × 1040 pixels with a pixel size manufacturer-calibrated to be 107.5 nm. The camera exposure was set to 10 ms and images captured at 11.05 focusing using Nikon's NIS

Elements software.

Collagen-coated slides

A chamber flow slide with a collagen IV coating (ibidi, μ-Slide I Luer $^{0.8}$) was used. The channel was carefully filled with the M13-aCol-TRITC construct sample and left to incubate for 1 h at room temperature. The slide was linked to the tubing ('white' perfusion set, #10963) of the pump system. Reservoirs were filled with PBS. The software allows varying the pressure/flow rate/shear stress to the desired testing values. A defined nominal shear stress (WSS on a flat surface due to the bulk flow rate) profile was applied, ranging from –3.5 to +3.5 dyn.cm^{-2}, lasting 20 seconds each cycle. The experiments were performed at 35 °C, on the temperature-controlled system box of the microscope. The reservoirs and tubing left inside the box for 1h to equilibrate the temperature of the buffer.

Endothelial-coated slides

The apparatus used for the collagen antibody constructs was also used for the cellular experiments. GEnCs were seeded onto the same type of flow collagen-coated slide (ibidi, μ-Slide I Luer$^{0.8}$) and the M13-WGA-TRITC construct was added to the chamber and left to react for 1h in an incubator at 37 °C. The slide was linked to the pressure pump and the reservoir of the fluidic unit was filled with PBS buffer. A defined nominal wall shear stress profile was applied, ranging from –3.5 to +3.5 dyn.cm^{-2}, lasting 20 seconds each cycle.

Probability model of M13 bacteriophage orientation in flow

The tethered fibre motion under Brownian effects and flow is modelled phenomenologically by a random walk with spatially homogeneous jump probability, but a spatially-varying difference in the probability of left or right jumps, modelling the biasing effect of the viscous restoring force. The partial differential function (PDF) $p(\varphi,t)$ was modeled on a one-dimensional grid $\{0,\pm\Delta\varphi,\pm 2\Delta\varphi,\ldots,\pm n\Delta\varphi\}$ with jump probabilities $k_{-}(\varphi)$ and $k_{+}(\varphi)$ having constant sum $(k_{+}+k_{-})$ and their difference $(k_{+}-k_{-})$ varying with angle φ, corresponding to the increase in restoring viscous stress with deviation from the flow direction.

The discrete random walk model can be written down by considering respectively the probabilities that a fibre will jump from the left, will stay where it is, or will jump from the right, over a time period $[t,t+\Delta t]$

$$\begin{aligned} p(\varphi,t+\Delta t) = {} & p(\varphi-\Delta\varphi,t)k_{+}(\varphi-\Delta\varphi)\Delta t \\ & + p(\varphi,t)\left(1-\left[k_{+}(\varphi)+k_{-}(\varphi)\right](\Delta t)\right) + p(\varphi+\Delta\varphi,t)k_{-}(\varphi+\Delta\varphi)(\Delta t) \end{aligned} \tag{4}$$

A constant diffusion coefficient and a bias function $U(\varphi)$ in terms of the jump probabilities were defined as follows:

$$D=(\Delta\varphi)^2\frac{(k_{+}-k_{-})}{2} \tag{5}$$

$$U(\varphi)=(\Delta\varphi)(k_{+}-k_{-}) \tag{6}$$

Substituting for k_{+} and k_{-} and taking the limits as $\Delta\varphi\to 0$ and $\Delta t\to 0$ yields the partial differential equation,

$$\frac{\partial p}{\partial t}=D\frac{\partial^2 p}{\partial\varphi^2}-\frac{\partial}{\partial\varphi}Up \tag{7}$$

A steady state solution is expected to be valid because of the over-damped very low Reynolds number nature of the flow. Thus

$$\frac{\partial p}{\partial t}=0 \tag{8}$$

and hence

$$p = p(\varphi) \tag{9}$$

For situations physically symmetric about the flow direction $\varphi = 0$, the PDF must also be symmetric about $\varphi = 0$ yielding the boundary condition For situations physically symmetric about the flow direction $\varphi = 0$, the PDF must also be symmetric about $\varphi = 0$ yielding the boundary condition $\partial p / \partial \varphi(0) = 0$. p is also required to integrate to 1 and is 2π periodic. An approximate solution valid for small φ will give an easily-interpretable closed-form solution.

While we do not have an explicit form for $U(\varphi) = 0$, without detailed fluid dynamical modeling, it is clear that $U(0) = 0$, *i.e.* there is no restoring viscous force when the fibre is aligned with the flow direction, and that the fibre is aligned with the flow direction and that $U'(0) < 0$ so that the force does indeed bias the fibre towards alignment. At leading order therefore $U \approx \beta\varphi$ for some positive constant β which depends on shear rate.

While we do not have an explicit form for $U(\varphi) = 0$, without detailed fluid dynamical modeling, it is clear that $U(0) = 0$, *i.e.* there is no restoring viscous force when the fibre is aligned with the flow direction, and that the fibre is aligned with the flow direction and that $U'(0) < 0$ so that the force does indeed bias the fibre towards alignment. At leading order therefore $U \approx \beta\varphi$ for some positive constant β which depends on shear rate. These assumptions lead to the Ordinary Differential Equation,

$$0 = D\frac{d^2 p}{d\varphi^2} + \frac{d(\beta\varphi p)}{d\varphi} \tag{10}$$

which has solution

$$p = A\exp\left(\frac{-\beta\varphi^2}{2D}\right) \tag{11}$$

i.e. a normal distribution with mean 0 and variance □/□. Given that viscous drag at very low Reynolds number is linear in fluid velocity, it follows that the standard deviation of p, σ, will be proportional to the inverse square root of the shear rate.

$$\sigma^2 \propto \frac{1}{WSS \cdot M} \tag{12}$$

where M is the material time constant which is essentially the inverse rotational diffusion constant so proportional to L^3 for a slender rod of length L [4]. Thus

$$\sigma^2 \propto \frac{1}{WSS \cdot L^3} \tag{13}$$

so

$$\ln(\sigma) = -0.5\ln(WSS) - 1.5\ln(L) + k \tag{14}$$

where k is a constant. The full data plot for the collagen-coated slides is given in Fig. SI1.

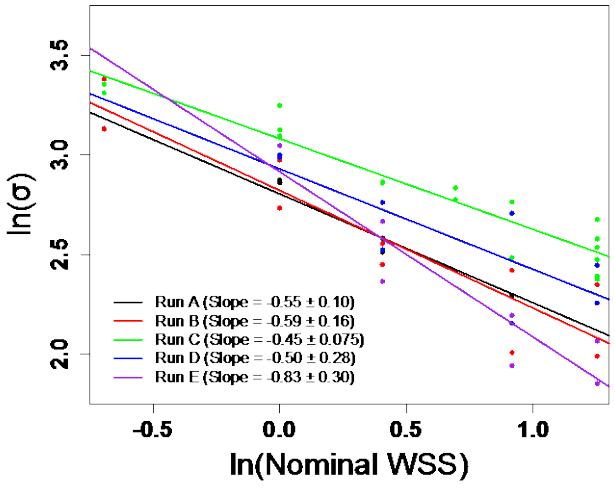

Figure SI1 ln(σ) versus ln(nominal WSS) 5 measured ColIV-M13-TRITC movies, for σ the standard deviation of the angle at each flow rate.

Movies of M13 bacteriophage in flow

Movie SI1: Movie of behaviour of M13- aCol-TRITC bound to a collagen IV coated flow slide (Fig. 3 Run A). The movie is approximately 4× real-time speed.

Movie SI2: Movie of behaviour of M13-WGA-TRITC bound to the surface of a cultured endothelial cell (Fig. 2(b) and Fig. 4). The angles derived by our detection method are drawn over the M13 on the left and plotted in the chart. The same M13 with the angles drawn over measured by the directionality plugin (Fiji/ImageJ) is on the right. The movie is approximately 6x real-time.

References

[1] Ghosh, D.;Lee, Y.;Thomas, S.;Kohli, A. G.;Yun, D. S.;Belcher, A. M.; Kelly, K. A. M13-templated magnetic nanoparticles for targeted in vivo imaging of prostate cancer. *Nat. Nanotechnol.* **2012**, *7*, 677-682.

[2] Pacheco-Gomez, R.;Kraemer, J.;Stokoe, S.;England, H. J.;Penn, C. W.;Stanley, E.;Rodger, A.;Ward, J.;Hicks, M. R.; Dafforn, T. R. Detection of Pathogenic Bacteria Using a Homogeneous Immunoassay Based on Shear Alignment of Virus Particles and Linear Dichroism. *Anal. Chem.* **2012**, *84*, 91-97.

[3] Satchell, S. C.;Tasman, C. H.;Singh, A.;Ni, L.;Geelen, J.;von Ruhland, C. J.;O'Hare, M. J.;Saleem, M. A.;van den Heuvel, L. P.; Mathieson, P. W. Conditionally immortalized human glomerular endothelial cells expressing fenestrations in response to VEGF. *Kidney Int.* **2006**, *69*, 1633-1640.

[4] Kim, S.; Karilla, S. J. *Microhydrodynamics: Principles and selected applications*; Butterworth-Heinemann Boston, 1991.

Address correspondence to Alison Rodger. A.rodger@warwick.ac.uk